(12) INTERNATIONAL APPLICATION PUBLISHED UNDER THE PATENT COOPERATION TREATY (PCT)

(19) World Intellectual Property Organization
International Bureau

(43) International Publication Date
29 March 2012 (29.03.2012)

PCT

(10) International Publication Number
WO 2012/040223 A2

(51) **International Patent Classification:**
CI2Q 1/00 (2006.01)

(21) **International Application Number:**
PCT/US201 1/052390

(22) **International Filing Date:**
20 September 201 1 (20.09.201 1)

(25) **Filing Language:** English

(26) **Publication Language:** English

(30) **Priority Data:**
61/385,146 2 1 September 2010 (21 .09.2010) US

(71) **Applicant** *(for all designated States except US):* **NORTH CAROLINA CENTRAL UNIVERSITY** [US/US]; 1801 Fayetteville Street, Durham, NC 27707 (US).

(72) **Inventors; and**

(75) **Inventors/Applicants** *(for US only):* **SEXTON, Jonathan, Z.** [US/US]; 1801 Fayetteville Street, Durham, NC 27707 (US). **BRENMAN, Jay** [US/US]; 1801 Fayetteville Street, Durham, NC 27707 (US).

(74) **Agents: CORD, Janet, I.** et al; Ladas & Parry LLP, 1040 Avenue of the Americas, New York, NY 10018 (US).

(81) **Designated States** *(unless otherwise indicated, for every kind of national protection available):* AE, AG, AL, AM, AO, AT, AU, AZ, BA, BB, BG, BH, BR, BW, BY, BZ, CA, CH, CL, CN, CO, CR, CU, CZ, DE, DK, DM, DO, DZ, EC, EE, EG, ES, FI, GB, GD, GE, GH, GM, GT, HN, HR, HU, ID, IL, IN, IS, JP, KE, KG, KM, KN, KP, KR, KZ, LA, LC, LK, LR, LS, LT, LU, LY, MA, MD, ME, MG, MK, MN, MW, MX, MY, MZ, NA, NG, NI, NO, NZ, OM, PE, PG, PH, PL, PT, QA, RO, RS, RU, RW, SC, SD, SE, SG, SK, SL, SM, ST, SV, SY, TH, TJ,

[Continued on next page]

WO 2012/040223 A2

(54) Title: METHOD FOR TREATING NON-ALCOHOLIC FATTY LIVER DISEASE AND TYPE-II DIABETES

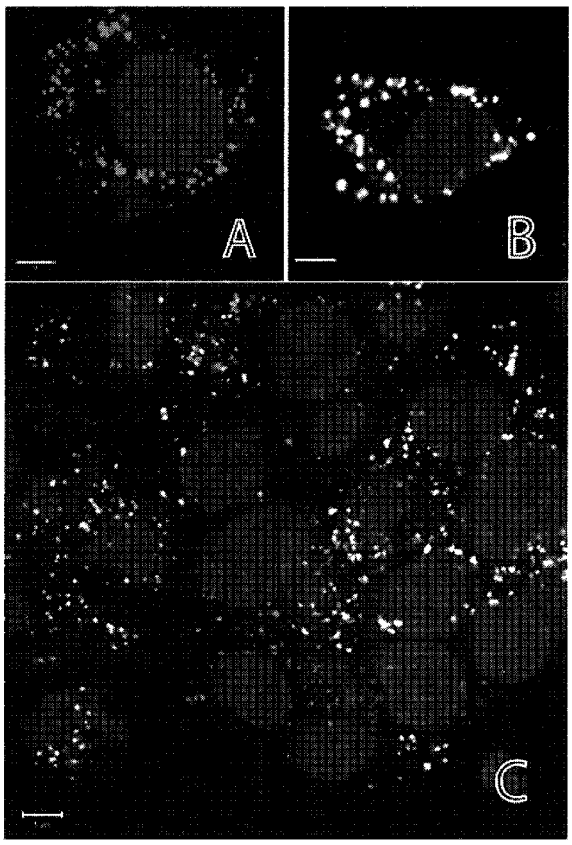

(57) Abstract: This relates generally to compounds that can be used to treat nonalcoholic fatty liver disease and type II diabetes and an assay for identifying the compounds. The invention also relates to an assay that can be used to identify compounds that increase cellular peroxisomal mass.

TM, TN, TR, TT, TZ, UA, UG, US, UZ, VC, VN, ZA, ZM, ZW.

(84) Designated States *(unless otherwise indicated, for every kind of regional protection available):* ARIPO (BW, GH, GM, KE, LR, LS, MW, MZ, NA, SD, SL, SZ, TZ, UG, ZM, ZW), Eurasian (AM, AZ, BY, KG, KZ, MD, RU, TJ, TM), European (AL, AT, BE, BG, CH, CY, CZ, DE, DK, EE, ES, FI, FR, GB, GR, HR, HU, IE, IS, IT, LT, LU, LV, MC, MK, MT, NL, NO, PL, PT, RO, RS, SE, SI, SK, SM, TR), OAPI (BF, BJ, CF, CG, CI, CM, GA, GN, GQ, GW, ML, MR, NE, SN, TD, TG).

Published:

— *without international search report and to be republished upon receipt of that report (Rule 48.2(g))*

METHOD FOR TREATING NON-ALCOHOLIC FATTY LIVER DISEASE AND TYPE-II DIABETES

This invention was supported in part by funds from the US. Government. The U.S. government may therefore have certain rights in the invention.

Field of the Invention

The present invention relates generally to compounds that can be used to treat nonalcoholic fatty liver disease and type II diabetes and an assay for identifying the compounds. The invention also relates to an assay that can be used to identify compounds that increase cellular peroxisomal mass.

Background of the Invention

Peroxisomes are ubiquitous eukaryotic organelles that carry out metabolic reactions and responses to cellular oxidative stress. Peroxisomes represent a major site of fatty acid β-oxidation and the only site of very long-chain fatty acid (VLCFA) β-oxidation in the cell. In addition to oxidizing fatty acids, peroxisomes help synthesize vital plasmalogens, special ether phospholipids that include sphingolipids, a major component of both myelin and lipid rafts. Sphingolipids are highly enriched in the nervous system while other plasmalogens (eg. choline plasmalogen) are uniquely enriched in the heart. The vital function of peroxisomes was made clear with the molecular identification of mutations in a peroxisomal biogenesis disorder (PBD) first identified in 1992 in humans. There are four fatal clinical disease syndromes associated with PBDs - Zellweger syndrome (ZS), neonatal adrenoleukodystrophy (NALD), infantile Refsum disease (IRD) and rhizomelic chondrodysplasia punctata (RCDP).

Therapeutically targeting peroxisome biogenesis follows from the hypothesis that increasing fatty acid oxidation capacity could be beneficial for many aspects of metabolic syndrome by decreasing lipotoxicity particularly in key metabolic tissues like the liver. The lipotoxicity hypothesis posits that elevated plasma fatty acids may lead to ectopic lipid accumulation in non-adipose tissue, particularly the liver ("fatty liver"), that harms organ and cellular function. In addition, consumers of

Western high-fat diets may benefit from increased fatty acid oxidation capacity as elevated plasma free fatty acids can contribute to insulin resistance and hyperglycemia, which are risk factors for both metabolic syndrome and T2D (type 2 diabetes). Indeed, it has long been known that many structurally unrelated compounds that increase peroxisome biogenesis in rodents are also successful in treating symptoms of dyslipidemia and metabolic syndrome (MetS) in rodents.

The fibrates (Clofibrate, Bezafibrate, Ciprofibrate, Gemfibrozil, and Fenofibrate) represent one class of plasma lipid lowering drugs commonly prescribed in the 1970s. Although the mechanism of fibrate action was not known at the time, researchers screening for a fibrate-like drug in a diabetic mouse model identified Ciglitazone, a thiazolidinedione ("glitazone") compound. Through Structure Activity Relationship (SAR) programs Ciglitazone gave rise to rosaglitazone (Avandia™) and pioglitazone (Actos™). Currently, fibrates are preferentially thought to activate peroxisome proliferator activated receptor a (PPARa) in the liver, while thiazolidinediones preferentially activate PPARy in adipose tissue for their therapeutic effects. Despite the original PPAR name, current marketed PPAR agonists, particularly the glitazones, do not increase peroxisome biogenesis in humans. However, multiple compounds structurally unrelated to fibrates display both hypolipidemic effects and peroxisome proliferation in rodents suggesting that peroxisome proliferation itself may produce beneficial effects, perhaps through increased fatty acid oxidation.

Experimental evidence further supports peroxisome biogenesis as potentially therapeutic since rodents treated with fibrates display increased peroxisome proliferation and both enhanced insulin sensitivity and reduced fat deposition in the obese Zucker rat model. Interestingly, fibrates also enhance fatty acid oxidation in both lean and obese Zucker rats. Although both fibrates and rosiglitazone lower serum triglycerides in fatty Zucker rats, only fibrates lower body weight, while rosiglitazone leads to large undesirable weight gains in adipose tissue, an effect also seen in humans. This suggests that novel approaches to increase peroxisome biogenesis in humans could be superior to current PPAR treatments for diabetes and metabolic syndrome. Indeed, it has recently been documented that the U.S. Food and Drug Administration (FDA) approved drug 4-phenylbutyrate (PBA), a PPAR independent peroxisome proliferator

and chemical chaperone, treats symptoms of MetS and T2D in ob/ob (obese diabetic) and db/db (diabetic) mice and in B6/HFD (high fat diet) mice, including restoration of glucose homeostasis, enhanced insulin sensitivity and decreased fatty liver disease. PBA is a non-classical PPAR-independent peroxisome proliferator. It serves as a positive control compound as a potent peroxisome proliferator in our human-liver cell line high throughput assay. Although PBA has been shown to be effective, it must be used at extremely high doses (1 g/Kg in rodents) and results in off-target side effects. PPAR-dependent compounds also display deleterious side effects (eg. FDA black box warning on rosiglitazone (Avandia™) and weight gain).

Compounds that promote peroxisome biogenesis with high potency *via* PPAR-independent mechanisms may represent attractive therapeutic chemical entities. No previous assay that the inventors are aware of has identified chemical comounds that can increase peroxisome biogensis in human cells in an high output screening (HTS) format. A novel genetically encoded peroxisomal reporter cell-line and a novel 3-channel high-content primary assay to identify compounds that increase cellular peroxisomal mass were developed.

Summary of the Invention

The present invention relates to a genetically encoded peroxisomal reporter cell line.

In addition, the present invention relates to an assay to identify compounds that increase cellular peroxisomal mass.

Another aspect of the invention is a high throughput screening assay to monitor peroxisome biogenesis in human cells.

Brief Description of the Drawings

Figure 1(A) shows enhanced peroxisome targeting fluorescent reporter (EPTFR) in HepG2 human cells.

Figure 1(B) illustrates double labeling of peroxisomal antigen PMP-70 (red) and EPTFR (Green) demonstrating co-localization. The general number, distribution and shape of peroxisomes is unchanged in EPTFR expressing cells (C, yellow). (Blue = Hoescht (nuclei)) (scale bar = 5 μm).

Figure 2(A) shows spectral multiplexing of Hoechst (blue), GFP, and CellTracker-Red fluorescent probes.

Figure 2 (B) is a flow cytometry analysis of a stable EPTFR-HepG2 line (green) and a wild-type HepG2 line showing suitability of the cell line for high-content screening purposes. The filled histogram shows a monophasic population of cells with substantial GFP expression (approximately 300x greater than the negative population). This cell population is sampled from the low-passage master cell-bank that was used in this screening effort.

Figures 3(A), 3(B) and 3(C) show PBA validation as a positive control for high content assay development and screening.

Figure 3(A) is a dose-response curve for GFP fluorescence (inset structure of PBA) exhibiting a 2.4 mM EC_{50}. PBA causes significant increases in peroxisomes visualized with EPTFR-HepG2 cells (blue - nuclei, green - peroxisomes) showing normal peroxisome distribution.

Figure 3(B) shows peroxisome with DMSO vehicle.

Figure 3 (C) shows increased peroxisomal content with PBA.

Figure 4 shows image segmentation showing Figure 4(A) merged color image with blue nuclei, red cytoplasm and green peroxisomes, Figure 4(B) nuclear binary mask, and Figure 4 (C) cytoplasmic mask. Each colored object in the masks indicates a unique cell, showing effective segmentation. Figure 4(D) shows

peroxisomes masked (red) with nuclei (blue), and Figure 4(E) assignment of peroxisomes to individual cells inside the respective cell mask.

Figure 5 shows Min-Max assay validation in two 384 well plates showing incubation with positive control (Max - 9.0 mM), and assay negative control (Min - DMSO carrier). The table shows assay statistics, resulting in a calculated Z of 0.72.

Figure 6 illustrates pilot screening results from the Prestwick FDA-approved drug library. Figure 6(A) shows pilot screen scatter for the 1120 compound Prestwick library. Response in this assay is calculated as a percent-effect as compared with the positive control. A cursory hit threshold is drawn at <32% effect, representing the $\mu + 3\sigma$ Figure 6(B) is a dose response confirmation for the active compound niclosamide (inset) showing a 2.4 μM EC50 and correlating western blot (left lane = DMSO, right lane = positive control) normalized to tubulin. Increased GFP expression correlates with increased peroxisomal specific antigen PMP-70 (†33%). U represents arbitrary fluorescent units.

Figure 7 shows production of HCA screening data for 15 k compounds for peroxisomal biogenesis. Figure 7(A) is a scatterplot for 15,000 compounds screened, Figure 7(B) is a histogram for the screen showing a normal (Gaussian) statistical distribution and Figure 7 (C) is a box plot for the screen showing distribution statistics and outliers (points).

Figure 8 shows 20χ color micrographs of Oil Red O staining of lipid droplets in HepG2 cells for untreated (Figure 8A) and PBA treated (Figure 8B) conditions showing a significant decrease in the size and intensity of staining with PBA. The respective histograms (lower panels) show the distribution of lipid droplet size per cell. Untreated mean lipid droplet area of -300 pixels2 (0.02 μιη2) compared 50 pixels2 (0.003 μm2) for PBA treated.

Figure 9 shows HepG2-peroxisomal response to Niclosamide.

Figure 10 shows oil red O staining of HepG2.

Detailed Description of the Invention

The initial phase of assay development to probe peroxisomer biogenesis was carried out using a genetically encoded fluorescent reporter system to determine whether the fluorescent reporter would co-localize with peroxisomers and if the reporter would respond to stimulus. Due to its past demonstration of robust peroxisomal plasticity, a liver-derived cell line human hepatocellular carcinoma (HepG2) was used. Liver cells represent ideal targets for peroxisome biogenesis regulation. In rodents, liver cells *in vivo* show the most peroxisome plasticity (the ability to increase peroxisome biogenesis). Also, the liver may be the most relevant physiological site for targeting lipid and glycemic disorders as the liver is a central effector of energy metabolism. Liver steatosis for instance occurs in many metabolic diseases and obesity and also contributes to insulin resistance.

A novel stable cell line for this high-content assay utilizing an enhanced peroxisome targeting fluorescent reporter (EPTFR) that expresses a green fluorescent protein (GFP) variant that labels peroxisomes was developed. The HepG2 cell line was genetically encoded with an enhanced peroxisome targeting fluorescent reporter (EPTFR) that expresses a GFP variant labeling peroxisomes in live cells. The reporter is based on a well-characterized carboxy terminal three amino acid peptide Peroxisome Targeting Sequence 1 (PTS1) motif sufficient to target polypeptides to the peroxisomal membrane. The EPTFR can be assayed in live or fixed cells by simple fluorescent methods in real time. Generally, an SKL (serine-lysine-leucine) peptide at the extreme carboxy terminus is sufficient; however, we have found through optimization/experimentation that adding a particular fourth amino acid (arginine-RSKL) increases targeting efficiency in human cells. Figure 1(A) shows enhanced peroxisome targeting fluorescent reporter (EPTFR) in HepG2 human cells.

The EPTFR reporter in this cell line co-localizes with antibody stains against endogenous peroxisomal antigens (Figure 1(B), and both HepG2 cells expressing or not expressing our peroxisomal reporter show the same morphologies and numbers of peroxisomes (Figure 1(C)). Figure 1 shows that the general number, distribution and shape of peroxisomes is unchanged in EPTFR expressing cells. The

stably GFP-transfected and wild type HepG2 cell lines were analyzed with flow cytometric analysis and have concluded that a spectrally resolved fluorescent probe set (Figure 2A) was analyzed in both the stable and wild type cell lines with flow cytometric analysis (Figure 2B), concluding that the stable (G418 selected) cell line is monophasic, has remarkable GFP intensity allowing for short microscopic exposure times, and is ideal for screening purposes. The cells analyzed in Figure 2(B) were sampled from the low-passage EPTFR-HepG2 master cell bank that was used for this screening effort to reduce the day-to-day biological variability when screening from actively growing culture.

Sodium 4-phenylbutyrate (PBA) is a fatty acid mimetic (Figure 3) that is approved by the U.S. FDA (marketed as Buphenyl) for the treatment of urea cycle disorders. PBA has recently been implicated as a therapeutic molecule for type 2 diabetes(T2D)/ metabolic syndrome (MetS) in mice and is a substantial non-PPAR peroxisome proliferator in both human cells *in vitro* and rodent liver *in vitro.* Figures 3(B) and 3(C) show confocal fluorescence images acquired on the Pathway 855 bioimager of normal peroxisomal distribution (negative control treated with DMSO vehicle) and under 9 mM PBA treatment, showing massive increase in total peroxisomal mass per cell. This is consistent with the previous study in human primary hepatocytes that showed large peroxisomal antigen increases with 1- 5 mM PBA. We validated 4-phenylbutarate as a positive control for this assay and also demonstrated that this screen is capable of identifying potent novel chemical probes by the identification and validation of niclosamide, which is 1000 times more potent that PBA.

We have also demonstrated that PBA provides dose/response activity for peroxisome biogenesis in the GFP reporter system (Figure 3A) consistent with previously demonstrated microscopy studies and western blots. This result provides proof-of-principle that the phenotypic end-point of non-classical peroxisome proliferation in human cell lines can be harnessed for high content imaging analysis and converted into high throughput screening (HTS) assays that provide new tools for discovery of chemical probes and potential therapeutics. A validated reporter cell-line that co-localizes and responds to stimulus is requisite for high-content assay

development proliferation in human cell lines can be harnessed for high content imaging analysis and converted into HTS assays.

Accurate feature extraction for individual cells enables the detection of meaningful phenotypic change. Our general strategy for image analysis is to calculate as many cellular features as possible and use multivariate data reduction techniques including principal component analysis and partial least squares regression, coupled with biological insight to identify meaningful phenotypic change. Bioimage data generated from this assay consists of a multiplexed set of three images (blue-nucleus, red-cytoplasm and green-peroxisomes) of a field of cells acquired in the well-center using a 20X microscope objective. Refinement of automated image preprocessing and segmentation parameters for quantization of cellular response have been performed to ensure fidelity over a wide range of cell densities, GFP expression ranges, and minor fluctuations in staining. This process involves careful acquisition of reference images for background subtraction, image pre-processing, cell detection/segmentation, and feature extraction (Figure 4). Figure 3 (C) shows increased peroxisomal content with PBA.

Figure 4 shows image segmentation showing Figure 4(A) merged color image with blue nuclei, red cytoplasm and green peroxisomes, Figure 4(B) nuclear binary mask, and Figure 4 (C) cytoplasmic mask. Each colored object in the masks indicates a unique cell, showing effective segmentation. Figure 4(D) shows peroxisomes masked (red) with nuclei (blue), and Figure 4(E) assignment of peroxisomes to individual cells inside the respective cell mask.

Image pre-processing was performed in the following two steps: 1) correction of background illumination variation using a shading algorithm for all channels to ensure a flat field for segmentation; and 2) 10-pixel rolling-ball background subtraction in the GFP-peroxisome channel to aid in the separation and quantitation of the individuals peroxisomes.

Segmentation starts with identifying the well-separated individual nuclei in the Hoechst image by first thresholding the background and then applying the watershed algorithm for edge detection based on interpreting a grayscale image as a

topographical surface. This topographical surface is then flooded from its minima using upper boundary conditions to detect the edges and effectively segment closely spaced nuclei. A binary nuclear mask is generated as shown in Figure 4(B). The nuclear mask is then used as the basis for generating the cytoplasmic mask. The edge-detection algorithm is then used to mask the boundary of each cell's cytoplasm area using the Cell Tracker-Red image. All quantification of peroxisomal number/attributes is done inside of the individual cell cytoplasmic mask as shown in Figure 4(E). Peroxisomal parameters for each cell were calculated inside the cytoplasmic mask and include the total integrated GFP intensity (representing total peroxisomal mass), peroxisomal number through sub-object counting and various shape/size attributes. These per-cell statistics were then compiled into a SQL database for visualization, statistical analysis and tabulation of screening results.

BD Attovision was used for cell detection, segmentation and quantification of peroxisomal and nuclear parameters. The first step for detection of individual cells using the nuclear/Hoechst channel used a shading algorithm to flatten the image background due to nonhomogeneous illumination. Automatic thresholding was performed, followed by an optimized water-shed algorithm to aid in separation of closely packed cells. A binary nuclear mask was generated by fitting a polygon to the perimeter of the remaining regions of interest (ROIs) for tabulation of nuclear fluorescent attributes for individual cells. The cytoplasmic mask was delineated by geometrically expanding the nuclear mask by 25 pixels (1 pixel = 0.31 μm) or until adjacent cell boundaries meet. The cytoplasmic binary mask was used to tabulate peroxisomal parameters on the GFP channel. Several GFP intensity and distribution moments were tabulated per cell to achieve a thorough phenotypic peroxisomal description. Spot-counting (sub-object counting) was also performed on the GFP channel inside the cytoplasmic mask to tabulate the number, size and density of peroxisomers per cell.

BD Image Data Explorer was used to generate a database table which contained cell-level results for an individual plate, that was directly imported into JMP8 (Statistical Analysis Software, Cary NC) for initial data exploration and visualization in

assay development, for principal component analysis transformation of cell-level data, and for calculation of well-averaged results.

Well-averaged biological results were merged with chemical structure information using ActivityBase (IDBS Software) and were stored in the IDBS Oracle database. Nonlinear regressions were performed to fit dose response curves using a four-parameter one-site dose-response with the XL fit software (IDBS software).

Initial studies on the EPTFR-HepG2 cell line involved tabulating the total GFP intensity per cell for positive and negative control treatments. It was observed there was significant overlap between positive and negative control GFP expression leading to poor assay statistics (Z-prime close to zero). The difference between positive and negative samples was visually apparent but simple fluorescence intensity integration within a cell was inadequate to score the complex visual phenotype of this assay. The primary screening assay was single-point (single concentration) in an inter-plate duplicate format. The calculated peroxisomal response per cell, and per well was averaged for duplicate data and was analyzed for agreement between assay plates. Hits are identified by using a standard deviation based hit-threshold (signal mean plus 3x or 6x the standard deviation in the compound data). Duplicate wells that are identified as active that have a substantial disagreement (> 15%) are manually inspected and a decision is made depending on the visual inspection whether the compound effect is significant. Typically upon disagreement, one of the wells contains a foreign object or is out of focus and can be easily triaged out of the hit list. Compounds that significantly reduce the number of cells per well, as compared to controls, are flagged as toxic/antiproliferative for future categorization.

Assay development was conducted with the EPTFR-HepG2 cell line in 384 well plates to identify optimal assay timing, staining conditions, imaging conditions and data analysis procedures to yield the most sensitive assay for the detection of compounds than can influence peroxisomal biology. We optimized protocols for plating, drug incubation, staining and imaging the EPTFR-HepG2 cell line in the Pathway 855 high-content bioimager (BD Biosciences, Rockville. MD) with multiplexing to spectrally resolve the fluorophores; 1) green fluorescent protein-susion

labeling peroxisomes; 2) Hoechst 33342 for labeling the nuclei (blue) and 3) Cell Tracker Red for labeling the cytoplasm. Excellent spectral resolution was obtained in the peroxisome, nuclear and cytoplasmic images for accurate binary masking and subsequent quantification of cellular responses (Figure 2A).

We have developed all image-processing pipeline to tabulate as many intensity/shape/size/distribution properties for each cell as necessary (currently -50 parameters are calculated per cell). Principal component analysis (PCA) is then used to reduce the dimensionality of the data while regressing against the variation in the compound concentration. In the conventional PCA approach, one makes linear combinations of the independent variables and mines for the combination that maximizes the variance in the data set. While performing PCA for analyzing peroxisomal biogenesis, a significant amount of the variance observed from cell to cell was due to natural variation and not due to the influence of the positive control PBA. In this case, the natural variability and the drug response were convoluted and a simple analysis of GFP intensity was quite misleading. We performed principal component regression, where we take the correlated independent variables (cell size, number of peroxisomes, size of peroxisomes, shape of peroxisome, etc.) and un-correlate them with standard PCA. Components of the PCI used for hit-identification are shown in Table 1.

TABLE 1

Parameter	Eigenvalue
GFP Intensity	0.52
GFP Granularity	0.39
GFP Sub Object Count PI	-0.01
Hoechst Intensity	0.34
Cell Tracker Red Intensity	0.44
GFP Densitometry Mean	0.52

The un-correlated principal components describing the total variability in the data set were taken and regressed against the compound concentration in the dose-response study. This has the effect of eliminating a majority of the natural variability by focusing

on the effects of the drug alone and uncorrelating independent variables (such as cell size and peroxisome number). This data reduction procedure was used during assay development to accurately characterize the effects of compounds during screening. Accurate feature extraction for individual cells enables the detection of meaningful phenotypic change. Our general strategy for image analysis is to calculate as many cellular features as possible and use multivariate data reduction techniques including principal component analysis and partial least squares regression, coupled with biological insight to identify meaningful phenotypic change.

Bioimage data generated from this assay consists of a multiplexed set of three images (blue-nucleus, red-cytoplasm and green-peroxisomes) of a field of cells acquired in the well-center using a 20X microscope objective. Refinement of automated image pre-processing and segmentation parameters for quantization of cellular response have been performed to ensure fidelity over a wide range of cell densities, GFP expression ranges, and minor fluctuations in staining. This process involves careful acquisition of reference images for background subtraction, image pre-processing, cell detection/segmentation, and feature extraction (Figure 4). We have also analyzed the plate-to-plate variation in typical triplicate assay plates and have found an average coefficient of variation (CV) of 4.1% and the day-to-day variation of less than 5%. Assessment of the initial quality of the assay from this Min-Max experiment results in a calculated Z-prime for individual plates at approximately 0.72 (Figure 5). Our Z-prime value indicates the robustness of the high-content cell-based assay for high-throughput screening. We are ultimately interested in identifying small molecule potentiators of peroxisome biogenesis that also increase peroxisomal function, which can be validated by multiple secondary (orthogonal) assays such as fatty-acid uptake and oxidation in the future.

The BRITE diversity library screened in this HCS effort consists of 33,600 compounds selected for chemical diversity from the 350,000 compound BRITE library, which was chosen for maximal diversity in chemical space using clustering tools

provided with MOE (Molecular Operating Environment, Chemical Computing Group Inc.) using multi-objective optimization. This library was generated by combinatorial chemistry synthetic routes and was a gift from Biogen-Idec in 2005.

Niclosamide was identified in the assay of this invention as a compound that increase peroxisome biogenesis. Figure 6B shows the dose response curve for niclosamide (a positive compound identified in the Prestwick pilot screen) exhibiting a 2.4 μM EC_{50} and a correlating western blot (insert) showing that, upon stimulation with niclosamide at the EC_{50} dose, there is a 33% increase in the peroxisomal specific antigen PMP-70 (peroxisomal membrane protein-70) indicating increased peroxisomal content. Importantly niclosamide has no known PPAR activity in multiple PPAR assays available in public databases and in the scientific literature. Thus, corroboration between the GFP reporter system and the western blot showing substantial increase in the peroxisomal antigen PMP-70 provides proof-of-principle that this assay is capable of identifying non-PPAR modulators of peroxisome biology.

Figure 9 shows HepG2- Peroxisomal response to Niclosamide shows that HepG2 cells that were treated with 2.5 micromolar of Niclosamide showed a significant increase in peroxisome content relative to the control.

The oil red 0 staining of HepG2 shows normal lipid accumulation of liver cells (untreated) and treated with Niclosamide showing significantly less lipid accumulation as a response to response to niclosamide treatment. (Figure 10.) This indicates an increase in fatty acid turnover. This also shows that niclosamide can be used to treat non-alcoholic fatty liver disease.

Based on these results, niclosamide may be used in a method of treating nonalcoholic fatty liver disease and/or T2D.

Based on these results, 4-phenylbutyrate may be used in a method of treating nonalcoholic fatty liver disease and/or T2D.

Niclosamide or other compounds identified in the assay may be administered therapeutically or prophylactically to treat nonalcoholic fatty liver disease.

Niclosamide may be administered therapeutically or prophylactically to treat non-alcoholic fatty liver disease associated with type II diabetes.

It may also be administered therapeutically or prophylactically to treat type II diabetes.

Niclosamide can be used to treat non-alcoholic fatty liver disease and type II diabetes.

Niclosamide can be therapeutic as a monotherapy or can be administered with other active agents such as Metformin.

Niclosamide or other compounds identified in the assay can be administered in a pharmaceutically acceptable form meaning that the carrier, diluent, excipients, and/or salt must be compatible with the other ingredients of the formulation, and not deleterious to the recipient thereof. Pharmaceutically acceptable also means that the compositions, or dosage forms are within the scope of sound medical judgment, suitable for use for an animal or human without excessive toxicity, irritation, allergic response, or other problem or complication, commensurate with a reasonable benefit/risk ratio.

There are several experiments that should be performed once new compounds have been identified in the primary HTS screen before testing these compounds in animal models *in vivo.* Initially, secondary screens should be conducted using primary liver cells. Secondary assays should also be performed to establish that novel peroxisome modulators function in the absence of the EPTFR reporter: for instance by simple use of anti-peroxisomal immunocytochemistry or Western blot. Exclusion of compounds that directly activate PPARs should also be performed using commercial PPAR-activation assays. In addition, primary liver cells or liver cell lines from other species (including rodents) should also be utilized to test peroxisome

biogenesis compounds for conserved function as an important step before testing these compounds in rodent models *in vivo.*

Of the 10 compounds identified, we have identified two promising scaffolds that were multiply represented and appear to have good medicinal chemistry properties and potencies between 2 μM and 25 μM. The confirmation rate was relatively low at 48%, however many of the compounds that did not confirm had an upward trend at higher concentrations. Had the dose-response concentration been extended to 100-200 μM, we most likely would have observed greater than 50% effect. We chose to exclude these compounds from future study due to low potency. Several of the unconfirmed compounds were sufficiently cytotoxic (measured by the reduction in cell count per well as compared with the negative control wells) but were included in the event that they were very potent and cytotoxicity at the screening concentration might prove to be irrelevant. It is possible that compounds that interfere with processes that lead to peroxisomal turnover (eg, pexophagy or autophagy) can increase peroxisomal content. These compounds would likely cause cellular stress/cytotoxicity and would be observed through a reduction in total cell count per well as compared with negative control wells. Alternatively, these compounds could be eliminated from future study if they lead to decreased autophagic flux in secondary assays.

Peroxisome biogenesis disorders

It is possible that compounds identified herein could eventually lead to therapeutics either for treatment of PBDs or other metabolic disorders. Independent genetically defined mutations affecting peroxisomes result in a range of phenotypes in humans from specific peroxisomal enzyme deficiencies to the complete absence of peroxisomes depending on the molecular lesion. In the most extreme cases, complete absence of peroxisomes results in death within the first year of life (severe Zellwegers), while many other PBDs result in neurodegenerative-like conditions later in life. For investigators modeling human PBDs in the mouse, compounds that inhibit peroxisome biogenesis could be used as chemical tools to provide an alternative to laborious, time-consuming mouse genetic knockouts to model disease. Mouse gene knockout models have been made for selected PEX genes, however, mouse knockouts without

functioning peroxisomes die near birth making them a useful model only for the most severe PBDs. Compounds that inhibit peroxisome biogenesis that could be given at any time point - acutely or chronically - in the adult animal could be useful tools to model less severe forms of peroxisomal diseases and to elucidate normal contributions of peroxisomes for maintaining health and metabolism. In addition to fatty acid and VLCFA metabolism, peroxisomes are a major site of reactive oxygen species (ROS) inactivation and thus provide beneficial protection against free radicals. Peroxisomal catalase decomposes hydrogen peroxide while other peroxisomal enzymes metabolize harmful reactive oxygen species in the cell. Further, another function of the peroxisome is retroconversion of VLCFAs to docosahexaenoic acid (DHA) (found in fish oil), which may mediate numerous beneficial effects of very long chain n-3 (ω-3) fatty acids for treating cardiovascular disease including reduced mortality and myocardial infarction. Indeed, DHA synthesis is impaired in ZS fibroblasts lacking peroxisomes and DHA is also believed to have a required role in brain development and nervous system function. These other beneficial capacities of peroxisomes-increased free radical/reactive oxygen species inactivation and production of beneficial fatty acids (distinguish the fatty acid oxidation in peroxisomes from that of mitochondria). Although mitochondria are major sites of fatty acid oxidation, mitochondria also produce toxic entities through oxidative phosphorylation and are known to lead to the induction of apoptosis through the release of cytochrome c , which can lead to activation of capases and apoptosis. In this regard increasing fatty acid oxidation through peroxisomal rather than mitochondria biogenesis could in theory produced larger net benefits.

Although we hypothesize that novel compounds promoting peroxisomal activity independent of PPARs may provide treatments for metabolic disorders by preventing lipid accumulation in non-adipose tissue and decreasing fatty acids in plasma, these compounds need to be tested both in primary liver cells as well as *in vivo* in mice, including the high fat diet (HFD) diet induced obesity (DIO) model in mice. 4-phenylbutryate (PBA) is a PPAR independent compound that functions as a positive control for peroxisome biogenesis in this high content assay and has been demonstrated to be therapeutic in diabetic/ obese (ob/ob and db/db) mice. Thus the roadmap for

testing these compounds is well established. The underlying peroxisome biogenesis machinery is largely conserved.

Although we hope that non-PPAR peroxisome proliferators may have therapeutic value for MetS and T2D, there are other applications for small molecules that increase peroxisome biogenesis. These compounds could be used as chemical probes to identify their targets, perhaps elucidating new machinery regulating peroxisome formation not previously known. Yeast undergo massive peroxisome proliferation from single to hundreds of peroxisomes per cell when fatty acids are the sole nutrient source instead of sugars and thus have even greater proliferation than mammals. Forward genetic screens in yeast have indeed identified a series of mutations in conserved "PEX" (PEroXin) genes required for peroxisome biogenesis. The importance of this conserved machinery is evidenced by human mutations in 13 different conserved PEX genes that cause ZS, NALD, IRD or RCDP. Although most of the peroxisomal biogenesis genes are conserved from yeast to man (20 genes) the upstream transcriptional regulation of these genes cannot be conserved as yeast have no PPAR-like genes to regulate transcription.

Example 1

The HepG2 cells were cultured according to the ATCC guidelines with EMEM growth medium (ATCC# 30-2003), supplemented with 10% FBS, 1% P/S and 400 μg/ml G418. The HepG2/GFP stable cell line was expanded to generate a master cell bank for high-content screening. Cryogenically preserved stocks were made at the same passage number with approximately 1×10^6 - cells per 1 mL tube in cryo-preservation media consisting of growth media supplemented with 5% DMSO. 4-phenylbutyrate was used as the positive control in both single-point and dose-response studies and a 450 mM aqueous stock solution was prepared by dissolving 4.1 1 g 4-phenylbutyric acid (PBA. 99%, Sigma # P21005-25G, FW 164.2) in 35 mL of

autoclaved ddH_20 . This solution was titrated with an equimolar amount of 1 N NaOH (approximately 20.4 mL) to pH 7.0 to form the sodium salt.

The peroxisomer biogenesis assay was developed in 384-well format with a final assay volume of 50µL. 384-well Corning black/clear thin-bottom tissue-culture-treated imaging plates (Corning #3712) were coated with a solution of 50µg/mL Poly-D-lysine (Sigma-Aldrich) to aid in cell adherence overnight at 4°C, then washed twice with ddH_20 and air-dried.

Cells were thawed from freezer-stocks, counted using a Vi-Cell XR (Beckman-Coulter, Brea, CA) and diluted to a final concentration of 0.16 x 10^6 viable-cell/mL. 20µL of prewarmed growth medium were added to each well using a Mutidrop-384 (Thermo/ Fisher) with a sterile head before transferring 20 µL of cell suspension (3200 viable cells/well) into each well. The pre-addition of 20 µL of media prior to dispensing the cell solution dramatically improved the distribution of cells within the well, yielding a homogenous cellular distribution across the center of the well. The cell plates were then allowed to attach overnight in the incubator.

Compound addition

An intermediate dilution step was used to limit the overall DMSO exposure to below 1%. Intermediate dilution plates were made by adding 40 µL of growth media to the spotted compound plates as described herein and transferring 10 µL from this plate to two identical cell-plates in inter-plate duplicate format using the Biomek-NX workstation yielding a final single-point screening concentration of 2.5 µM and dose/response top concentration of 19.5 µM in 50 µL total assay volume. The plates were then incubated with compounds for three days. 4-phenylbutyrate was used as the positive control and 4.5 µL of a 450 µM stock solution was added to columns 23 and 24 of the intermediate dilution plates manually with an 8-channel P20 pipette. A final concentration of 9.1 mM 4-phenylbutyrate was achieved with the 10 µL transfer from intermediate dilution plate to cell plate.

Staining and fixation

Approximately 40 µL of media with compound was removed from each well using the Biomek NX workstation leaving enough liquid behind to wet cells. 30 µL of 10 µg/mL Hoechst-33342 and 2 µM Cell Tracker-Red (Invitrogen, Carlsbad, CA) were dissolved in media (omitting serum and antibiotics) and was added to each well and then incubated for 4.5 min at 37°C. 30µL of media was aspirated to remove excess dye and was replaced with 30 µL of fresh 4% formaldehyde. The cell plates were incubated in fixative for 45 min at 37°C. The cells were then washed once with PBS using the Biomek-NX at the slowest dispense speed and were sealed with Thermo-ABgene plate sealer and were imaged on BD Pathway 85 bioimager (Becton Dickenson, San Jose CA) within 2 hours of processing.

Immunohistocheniical staining

Colocalization studies

HepG2 Cells were cultured on cover slips, fixed with 4% formaldehyde and made permeable with 0.5% Triton X-100 in PBS for 10 min. Nonspecific binding was reduced by blocked in 3% BSA in PBS containing 0.5%, Triton X-100 for 30 min at room temperature. Cells were incubated with the primary rabbit anti-PMP 70 antibody (Sigma, 1:200 dilution) for 2 hours at room temperature. The secondary Goat anti-rabbit IgG conjugated with the Cy3 probe (1:200 dilution) was used for fluorescent labeling. Cover slips were mounted on glass slides using VECTASHIELD Mounting Medium with DAPI. The slides were imaged and analyzed using a BD Pathway-855 and Nikon Al confocal microscope for co-localization studies.

Lipid droplet staining

Oil-Red-O staining was performed on cover slip mounted HepG2 cells. Cells were allowed to attach on cover slips overnight, the media was removed and cells were fixed with 10% cold formalin (4% formaldehyde) for 10 minutes at room temperature. Cells were then washed in PBS twice and air-dried for 20 minutes. Slides were placed in 100% propylene glycol for 2 minutes and were stained with a 0.5% w/v Oil-Red-0 solution in propylene glycol for 10 minutes at 60°C. Slides were then differentiated in 85% propylene glycol in ddH_20 for 2 minutes, then rinsed twice in ddH_20 and stained

with Mayer's hematoxylin (diluted 1:2 in water) for 30 seconds. Cover slips were washed in running tap water followed by a ddH_20 rinse and then mounted with aqueous mounting media (10% glycerol in water). Cells were imaged with an Olympus bright-field microscope at 20X magnification with a 4 mega pixel color CCD camera and lipid droplets appear red in color and the nuclei appear pale blue.

Fluorescent imaging

The BD Pathway 855 was used to acquire multiplexed epifluorescent images in 384-well format with a 20X/0.7 NA Olympus UApo objective lens using the BD Attovision software. Green fluorescent protein labeled peroxisomes were imaged with a 481/10 nm band-pass excitation filter. Fura/FITC epifluorescence dichroic and a 515 nm long-pass emission filter. Hoechst dye labeled nucleic acids were imaged with a 380/10 nm band-pass excitation filter, a 400 nm dichroic long-pass, and a 435 nm long-pass emission filter. Laser-based autofocus was performed in each well prior to the collection of GFP and Hoechst images. Batches of six plates were processed and imaged at a time. Exposure times for both the GFP and Hoechst channels were adjusted prior to each batch to ensure optimal sigma-to-noise ratio.

Quantitative western blot analysis

Peroxisome content was assessed by normalizing the PMP-70 signal to the alpha-tubulin signal to control for variation in sample loading. HepG2 cells were seeded at a density of 5×10^5 cells in 6-well dishes in complete growth medium and were allowed to attach overnight. Compounds were delivered at the appropriate concentration in DMSO (while maintaining less than 1 % total DMSO concentration), and were allowed to incubate for 3 days. Cells were harvested, washed with cold PBS and total protein was extracted in lysis buffer (100 mM Tris-Cl pH 6.8, 2% SDS, I mM PMSF, Sigma protease inhibitor cocktail). Proteins were separated on 4%-12% NuPAGE BisTris gradient gels (Invitrogen) and then transferred to PVDF membrane. Blots were probed with a 1:3000 dilution of anti-PMP-70 and 1:16000 antialphatubulin (Sigma rabbit anti-PMP-70 and antialphatubulin clone B-5-1-2), followed with a 1:2000 dilution of secondary fluorescent antibodies (Li-Cor IRDye 680 Goat anti-rabbit and IRDye 800CW Goat anti-mouse). Western blot scanning and band quantification were

performed with the Odyssey infrared imaging system (Li-Cor Biosciences, Lincoln NE) according to the manufacturer's recommendations.

EC_{50} dose-response determination was performed in 384-well plates by cherry-picking 1 μl of compound from the corresponding 10 mM source plate, diluting to 5 μl total volume with DMSO for a final 2 mM compound concentration using a Biomek 3000 and P20 tips. Axygen conical 384-well PCR plates were used during the serial dilution scheme to facilitate mixing and small volume transfers. A 10-point 2-fold serial dilution was then performed across the plate with the Biomek® 3000. The serially diluted compounds were then spotted to columns 3-22 of a Greiner 384-well Polypropylene V bottom square well plate with the Biomek 3000 and P20 tips. Columns 1, 2, 23, and 24 were spotted with 0.5 μl of DMSO with the Biomek NX and P20 tips and used as positive and negative controls. A control dose response for PBA in wells A3-A12 for quality control purposes and measured 31 dose/responses per plate. Compounds that were confirmed with dose response were tested in intra-plate triplicate and cellular observations were averaged for each concentration and a single EC50 value was determined for each compound.

Assay validation

The assay was evaluated for screening robustness by performing a Min-Max experiment to determine the variance in the negative and positive controls. Ideally, the standard deviation in the cellular response will be small for all wells treated with a specific concentration of our positive control PBA , indicating a good signal-to-noise ratio (SNR) and a desirable Z-prime statistic (above 0.5).

Data from this Min-Max study show effective use of mM PBA concentration as a positive control in two 384-well plates with 0 mM and 9 mM (appropriate carrier solvent volume added to negative control) as shown in Figure 5. Each data point plotted in Figure 5 represents a well-averaged response demonstrating a suitable assay window (max-minus-min). The response (normalized peroxisomal response) is a linear combination of all measured peroxisomal attributes derived from partial least squares regression analysis and through rejection of a sub-population of cells that have a zero

detectable peroxisomes (less than 5% of the population). Assay conditions have been optimized to ensure that at least 100 cells per CCD field in a well with a 20X objective are captured to ensure adequate statistics even in the presence of anti-proliferative or cytotoxic compounds. Cells with less than one identifiable peroxisome were omitted from the analysis due to low potential for peroxisomal plasticity, further reducing variability in the assay.

Screening results

Pilot screen - FDA approved drug library

For concentration range-finding and to validate assay development parameters, we screened the commercially available Prestwick library, consisting of 1120 highly-diverse FDA-approved drugs that have established biological activities. Seven compounds were active from single-point screening (blue open diamonds in Figure 6A) and four were confirmed with dose/response in this assay, including niclosamide as shown in Figure 6B (inset), yielding an overall hit-rate of 0.4% and a confirmation rate of 66%.

Production screen - BRITE diversity set

15,360 compounds were screened for their ability to increase cellular peroxisome content and/or to significantly changing peroxisomal morphology. The normalized peroxisomal response (a linear combination of the most important peroxisomal parameters chosen from PCA analysis of the effects of PBA in the response including; GFP intensity, peroxisomal number per cell, cell size, nuclear content and peroxisomal shape statistics) is plotted for each compound as shown in Figure 7A. The screening data is transformed using the first principal component eigenvector, which reflects increases in the number and size of peroxisomes per-cell. The compound distribution data scatter as shown in the histogram and box plot in Figures 7B and 7C shows a normal (un-skewed) distribution with a mean set to zero and a standard deviation in compound data of 7.63, leading to a Z-factor = 0.63 and an overall Z-prime of 0.74 for this 15 k compound screen.

Dose response confirmation - EC50 determination

Of the 15 k compounds screened, 21 compounds were above a $\mu + 6\sigma$ threshold of 45 percent effect and were carried forward into dose-response studies yielding a primary hit rate of 0.14%. Of the 21 compounds tested in dose-response, 10 compounds exhibited dose-response behavior for a 48% confirmation rate. Of the compounds that did not confirm, several were trending upwards at 19.5 μM in the last or last-two data points but were not considered active due to low potency. Of the surviving 10 compounds, four were of the same scaffold with the most potent at 2 μM ECso. Two compounds from another promising scaffold were discovered and had potency between 10-20 μM. The remaining four compounds were structurally unrelated and have potencies ranging from 7-25 μM.

Decreased lipid droplet accumulation in HepG2 under 4-phenylbutyrate treatment

PBA treatment of diabetic mice resolves fatty liver and lowers liver triglyceride content. Treating HepG2 cells with PBA consistently decreased both the size and staining intensity of lipid droplets (Figure 8).

There is a left skew in the histogram of the untreated cells (Figure 8a lower panel). This non-Gaussian distribution is likely an artifact of the limited resolution of the chromogenic dye causing multiple distinct lipid droplets to appear superimposed. However, the peak of the distribution does accurately reflect the increased isolated lipid-droplet size. Decreases in numbers and sizes of lipid droplets generally reflect increased lipid catabolism as lipid droplets are the major triglyceride stores in eukaryotic cells. Although, more direct measures of compound-induced peroxisomal function will be pursued in the future, Oil-Red O staining provides a cheap, simple secondary assay to measure whether a compound crudely affects cellular lipid content.

References

1. Heymans HS, Schutgens RB, Tan R, et al. Severe plasmalogen deficiency in tissues of infants without peroxisomes (Zellweger syndrome). Nature 1983; 306(5938): 69-70. [PubMed: 6633659]

2. Shimozawa N, Tsukamoto T, Suzuki Y, et al. A human gene responsible for Zellweger syndrome that affects peroxisome assembly. Science 1992; 255(5048): 1132-1134. [PubMed: 1546315]

3. Song S. The role of increased liver triglyceride content: a culprit of diabetic hyperglycaemia? Diabetes Metab Res Rev 2002;18(1):5-12. [PubMed: 11921413]

4. Boden G. Fatty acid-induced inflammation and insulin resistance in skeletal muscle and liver. Curr Diab Rep 2006; 6(3):177-181. [PubMed: 16898568]

5. Reddy JK, Krishnakantha TP. Hepatic peroxisome proliferation: induction by two novel compounds structurally unrelated to clofibrate. Science 1975; 190(42 16): 787-789. [PubMed: 1 198095]

6. Fujita T, Sugiyama Y, Taketomi S, et al. Reduction of insulin resistance in obese and/or diabetic animals by 5-[4-(l-methylcyclohexylmethoxy) benzyl] -thiazolidine-2,4-dione (ADD-3878, U-63,287, ciglitazone), a new antidiabetic agent. Diabetes 1983; 32(9): 804-810. [PubMed: 6354788]

7. Willson TM, Brown PJ, Sternbach DD, et al. The PPARs: from orphan receptors to drug discovery. J Med Chem 2000; 43(4): 527-550. [PubMed: 10691680]

8. Guerre-Millo M, Gervois P, Raspe E, et al. Peroxisome proliferator-activated receptor alpha activators improve insulin sensitivity and reduce adiposity. J Biol Chem 2000; 275(22): 16638-16642. [PubMed: 10828060]

9. Clouet P, Henninger C, Niot I, et al. Short term treatment by fenofibrate enhances oxidative activities towards long-chain fatty acids in the liver of lean Zucker rats. Biochem Pharmacol 1990; 40(9): 2137-2143. [PubMed: 2242041]

10. Chaput E, Saladin R, Silvestre M, et al. Fenofibrate and rosiglitazone lower serum triglycerides with opposing effects on body weight. Biochem Biophys Res Commun 2000; 271(2): 445-450. [PubMed: 10799317]

11. Ozcan U, Yilmaz E, Ozcan L, et al. Chemical chaperones reduce ER stress and restore glucose homeostasis in a mouse model of type 2 diabetes. Science 2006; 313(5790): 1137-1 140. [PubMed: 16931765]

12. Ozcan L, Ergin AS, Lu A, et al. Endoplasmic reticulum stress plays a central role in development of leptin resistance. Cell Metab 2009; 9(1): 35-51. [PubMed: 19117545]

13. Basseri S, Lhotak S, Sharma A, et al. The chemical chaperone 4-phenylbutyrate inhibits adipogenesis by modulating the unfolded protein response. The Journal of Lipid Research 2009; 50(12): 2486-2501.

14. Gondcaille C, Depreter M, Fourcade S, et al. Phenylbutyrate up-regulates the adrenoleukodystrophy-related gene as a nonclassicai peroxisome proliferator. J Cell Biol 2005; 169(1): 93-104. [PubMed: 15809314]

15. Neuberger G, Maurer-Stroh S, Eisenhaber B, et al. Prediction of peroxisomal targeting signal 1 containing proteins from amino acid sequence. J Mol Biol 2003; 328(3): 581-592. [PubMed: 12706718]

16. Grabenbauer M, Satzler K, Baumgart E, et al. Three-dimensional ultra-structural analysis of peroxisomes in HepG2 cells. Cell Biochemistry and Biophysics 2000; 32(1): 37^19. [PubMed: 11330069]

17. Kobayashi K, Inoguchi T, Maeda Y, et al. The lack of the C-terminal domain of adipose triglyceride lipase causes neutral lipid storage disease through impaired interactions with lipid droplets. J Clin Endocrinol Metab 2008; 93(7): 2877-2884. [PubMed: 18445677]

18. Schrader M, Krieglstein K, Fahimi HD. Tubular peroxisomes in HepG2 cells: selective induction by growth factors and arachidonic acid. Eur J Cell Biol 1998; 75(2): 87-96. [PubMed: 9548366]

19. Baes M, Gressens P, Baumgart E, et al. A mouse model for Zellweger syndrome. Nature Genetics 1997; 17(1): 49-57. [PubMed: 9288097]

20. Gray RH, de la Iglesia FA. Quantitative microscopy comparison of peroxisome proliferation by the lipid-regulating agent gemfibrozil in several species. Hepatology 1984; 4(3): 520-530. [PubMed: 6586630]

21. Hoivik DJ, Quails CW Jr, Mirabile RC, et al. Fibrates induce hepatic peroxisome and mitochondrial proliferation without overt evidence of cellular proliferation and oxidative stress in cynomolgus monkeys. Carcinogenesis 2004; 25(9): 1757-1769. [PubMed: 1513101 1]

22. Srinivasan K, Ramarao P. Animal models in type 2 diabetes research: an overview. Indian J Med Res 2007; 125(3): 451^172. [PubMed: 17496368]

23. Schrader M, Fahimi HD. Mammalian peroxisomes and reactive oxygen species. Histochem Cell Biol 2004; 122(4): 383-393. [PubMed: 15241609]

24. Wang C, Harris WS, Chung M, et al. n-3 Fatty acids from fish or fish-oil supplements, but not alpha-linolenic acid, benefit cardiovascular disease outcomes in primary- and secondaryprevention studies: a systematic review. Am J Clin Nutr 2006; 84(1): 5-17. [PubMed: 16825676]

25. Ferdinandusse S, Denis S, Mooijer PA, et al. Identification of the peroxisomal beta-oxidation enzymes involved in the biosynthesis of docosahexaenoic acid. J Lipid Res 2001; 42(12): 1987-1995. [PubMed: 11734571]

26. Moore SA, Hurt E, Yoder E, et al. Docosahexaenoic acid synthesis in human skin fibroblasts involves peroxisomal retroconversion of tetracosahexaenoic acid. J Lipid Res 1995; 36(1 1): 2433-2443. [PubMed: 8656081]

27. Steinberg SJ, Dodt G, Raymond GV, et al. Peroxisome biogenesis disorders. Biochim Biophys Acta 2006; 1763(12): 1733-1748. [PubMed: 17055079]

1. A HepG2 cell line comprising an enhanced peroxisome targeting fluorescent reporter (EPTFR) that expresses a GFP variant labeling peroxisomes in live cells.

2. The cell line according to claim 1 wherein the EPTFR comprises a carboxy terminal three amino acid peptide Peroxisome Targeting Sequence 1 (PTS1).

3. The cell line according to claim 1 wherein the EPTFR comprises arginine- RSKL.

4. A method for identifying compounds that increase peroxisome biogenesis comprising adding a compound to the cell line of claim 1 and measuring peroxisome biogenesis.

5. An assay comprising the cell line of claim 1 and a means for measuring peroxisome biogenesis.

6. An assay comprising the cell line of claim 1 and a means for measuring cellular peroxisomal mass.

FIGURE 1

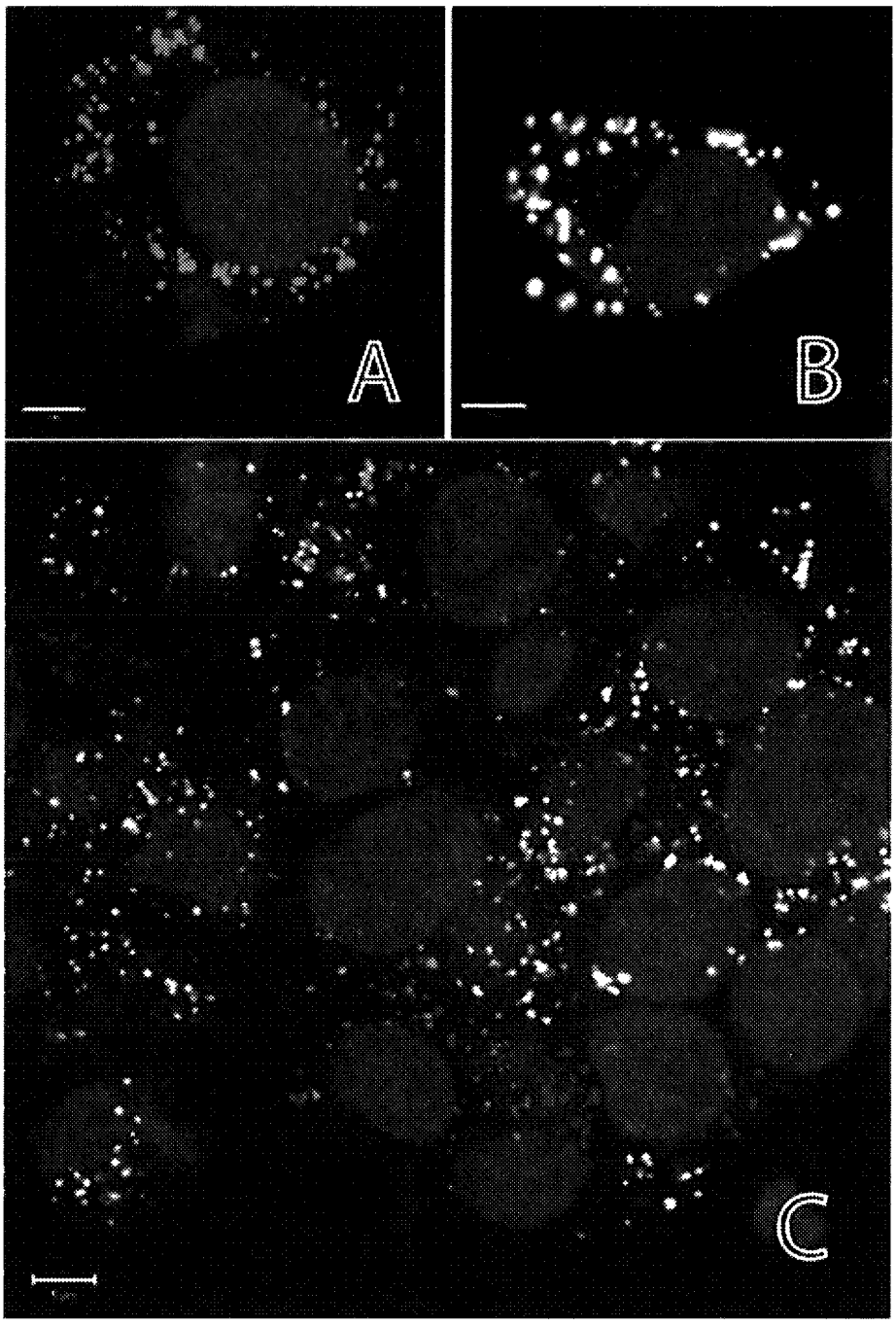

FIGURE 2

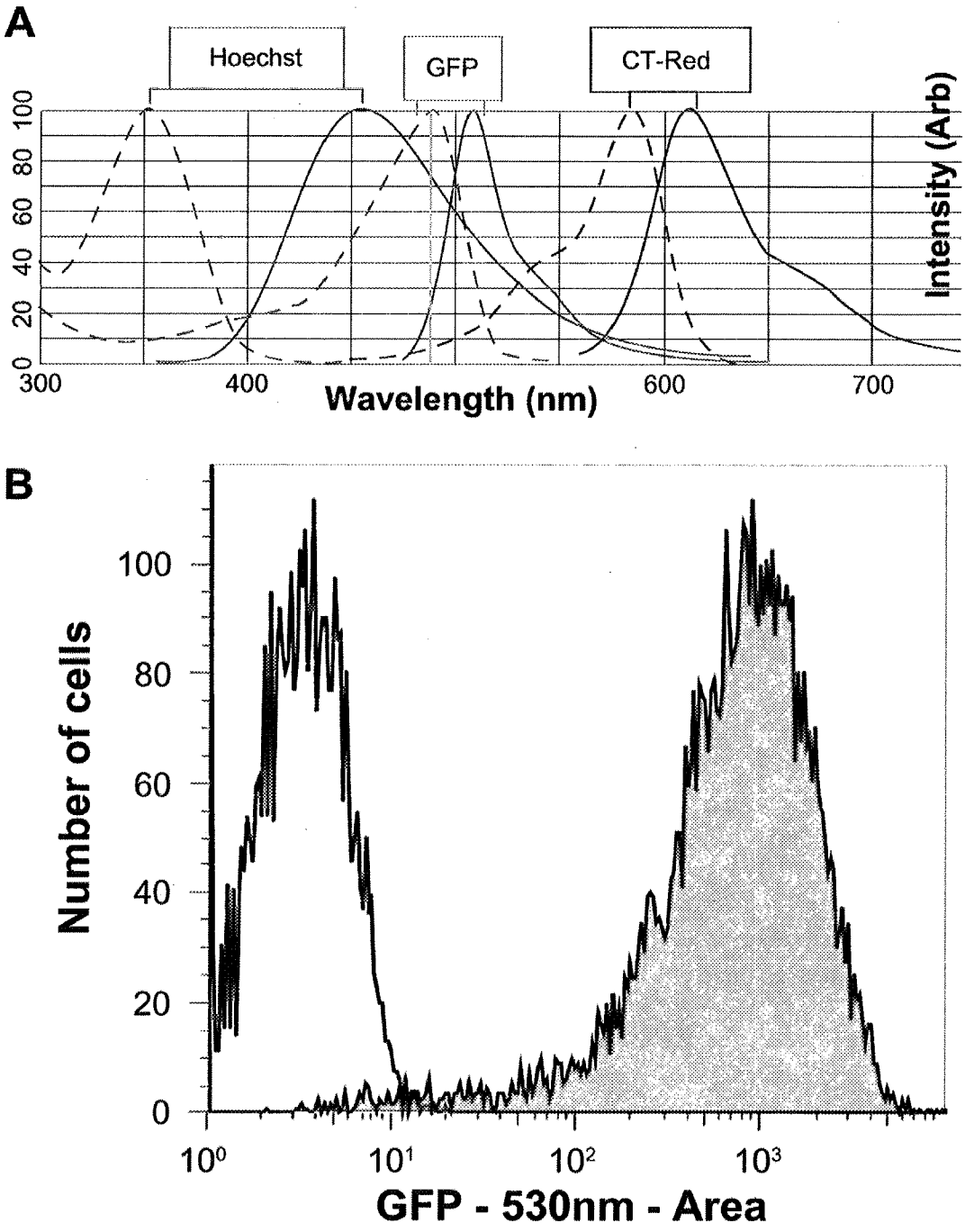
A
Hoechst
GFP
CT-Red
Intensity (Arb)
0
20
40
60
80
100
300
400
600
700
Wavelength (nm)
B
Number of cells
0
20
40
60
80
100
10^0
10^1
10^2
10^3
GFP - 530nm - Area

FIGURE 3

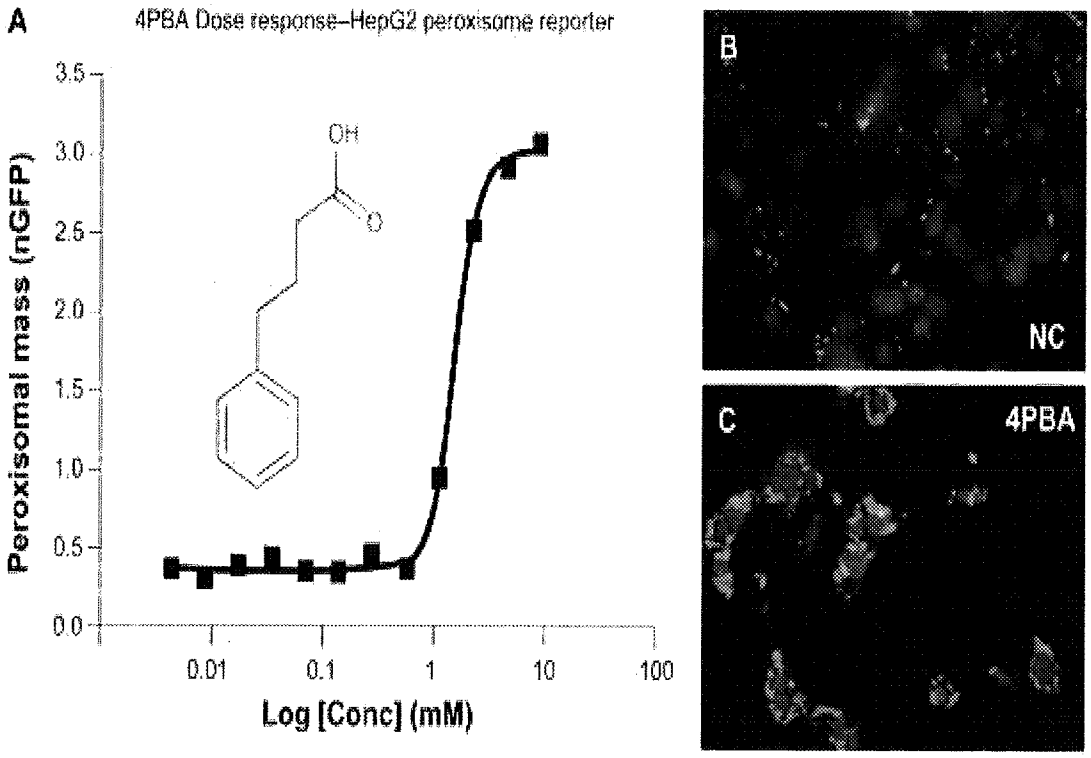
A
4PBA Dose response–HepG2 peroxisome reporter
Peroxisomal mass (nGFP)
3.5
3.0
2.5
2.0
1.5
1.0
0.5
0.0
OH
O
0.01
0.1
1
10
100
Log [Conc] (mM)
B
NC
C
4PBA

FIGURE 4

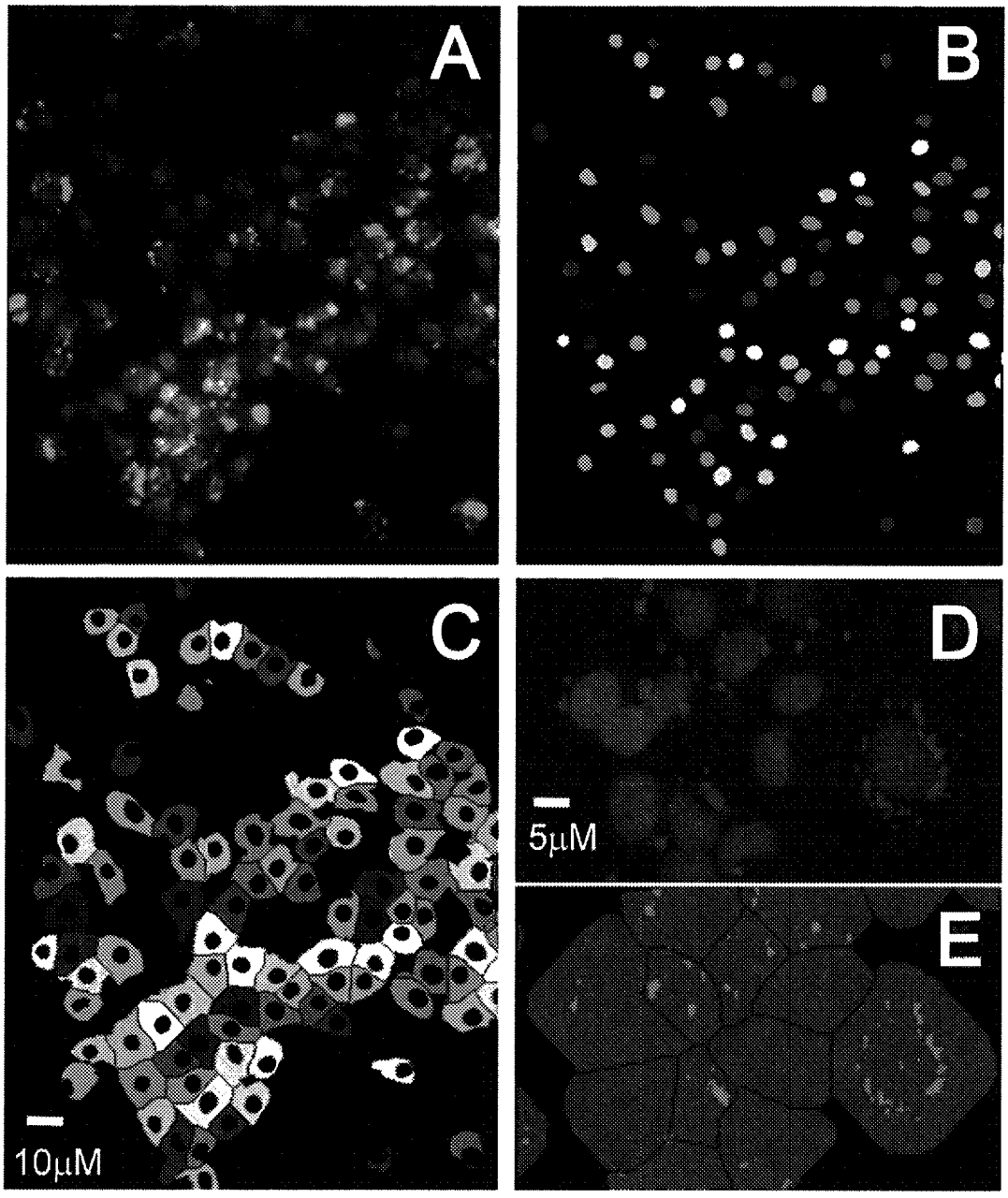

FIGURE 5

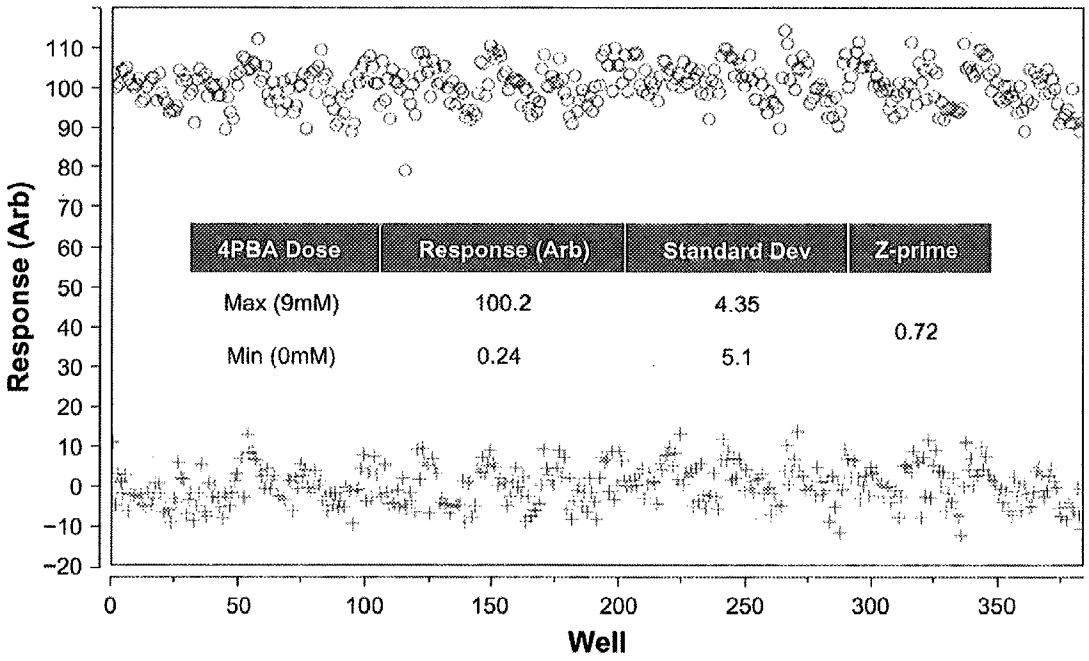
Response (Arb)
110
100
90
80
70
60
50
40
30
20
10
0
−10
−20
0
50
100
150
200
250
300
350
Well
4PBA Dose
Response (Arb)
Standard Dev
Z-prime
Max (9mM)
100.2
4.35
0.72
Min (0mM)
0.24
5.1

FIGURE 6

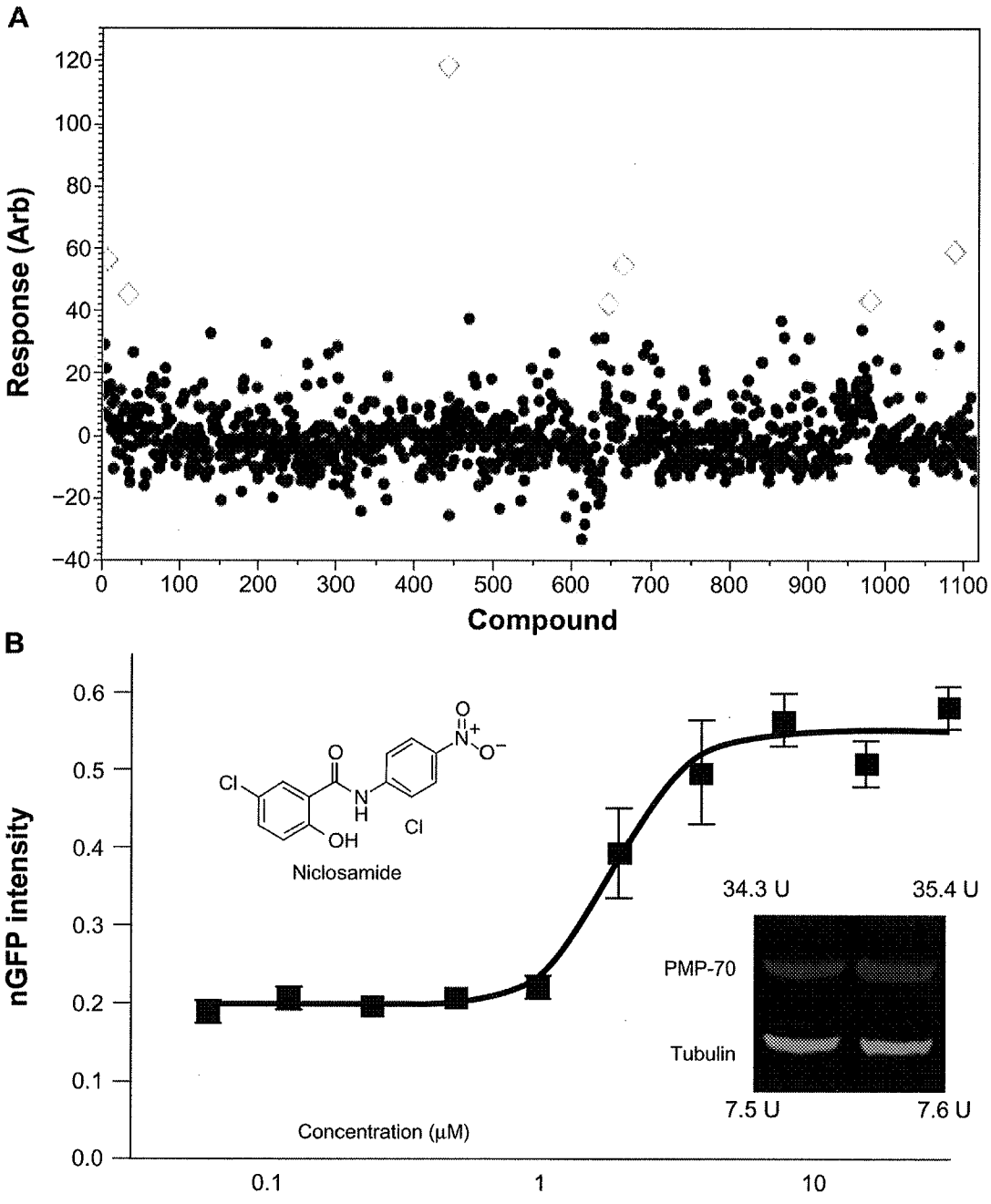
A
Response (Arb)
120
100
80
60
40
20
0
−20
−40
0
100
200
300
400
500
600
700
800
900
1000
1100
Compound
B
nGFP intensity
0.6
0.5
0.4
0.3
0.2
0.1
0.0
Cl
O
N
H
Cl
OH
O
N+
O−
Niclosamide
34.3 U
35.4 U
PMP-70
Tubulin
7.5 U
7.6 U
Concentration (μM)
0.1
1
10

FIGURE 7

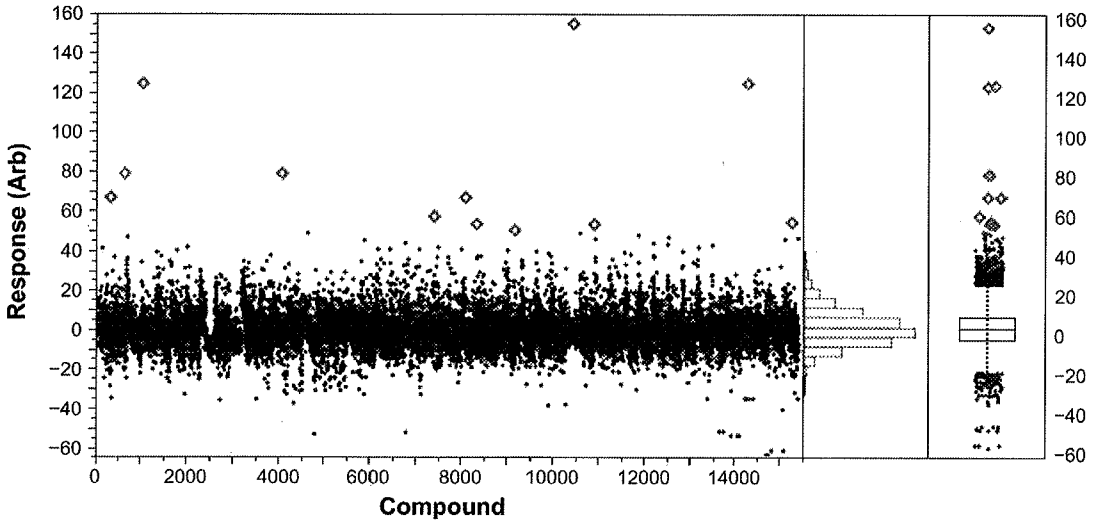
Response (Arb)
160
140
120
100
80
60
40
20
0
-20
-40
-60
0
2000
4000
6000
8000
10000
12000
14000
Compound

FIGURE 8

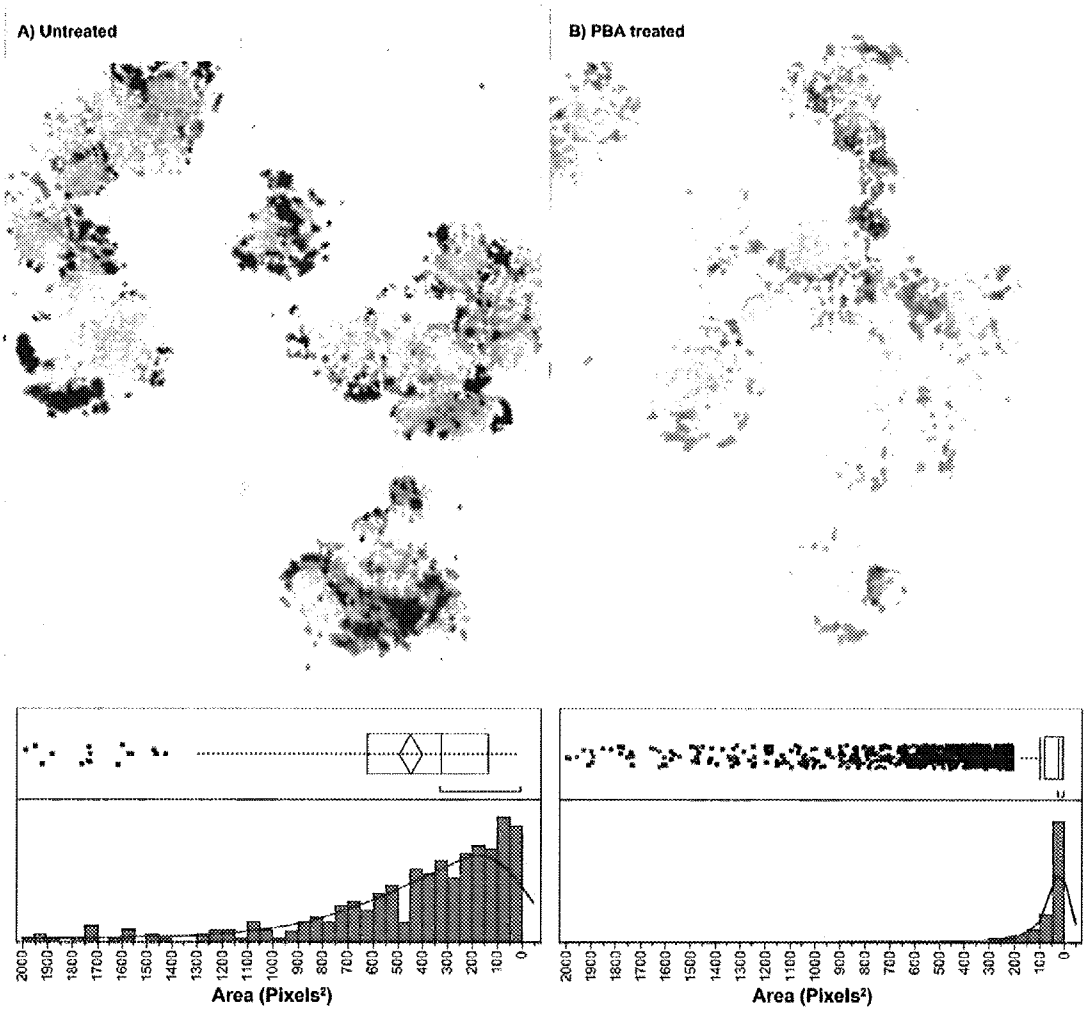
A) Untreated
B) PBA treated
2000
1900
1800
1700
1600
1500
1400
1300
1200
1100
1000
900
800
700
600
500
400
300
200
100
0
Area (Pixels²)
Area (Pixels²)

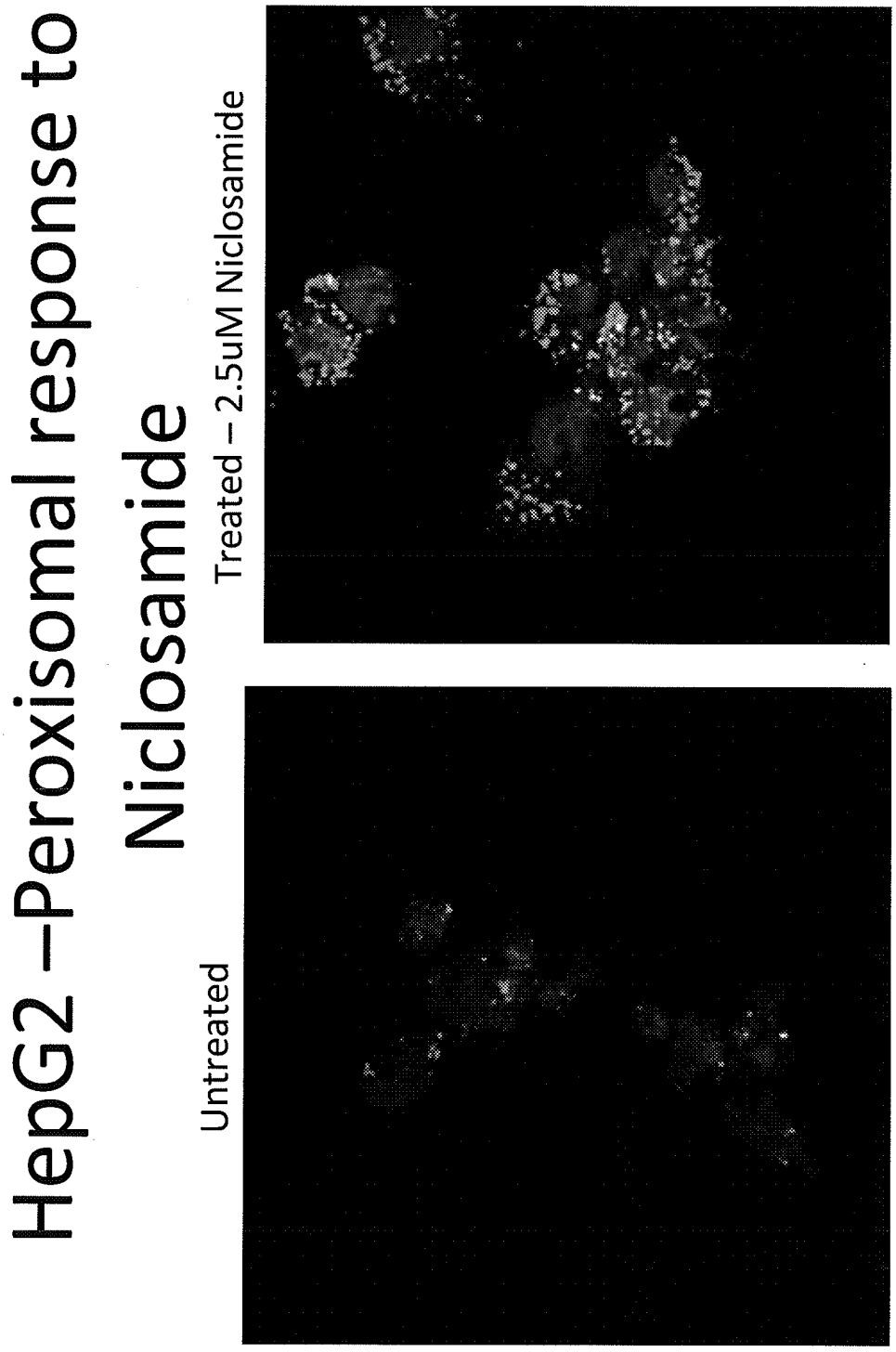
HepG2 –Peroxisomal response to Niclosamide
Treated – 2.5uM Niclosamide
Untreated

FIGURE 9

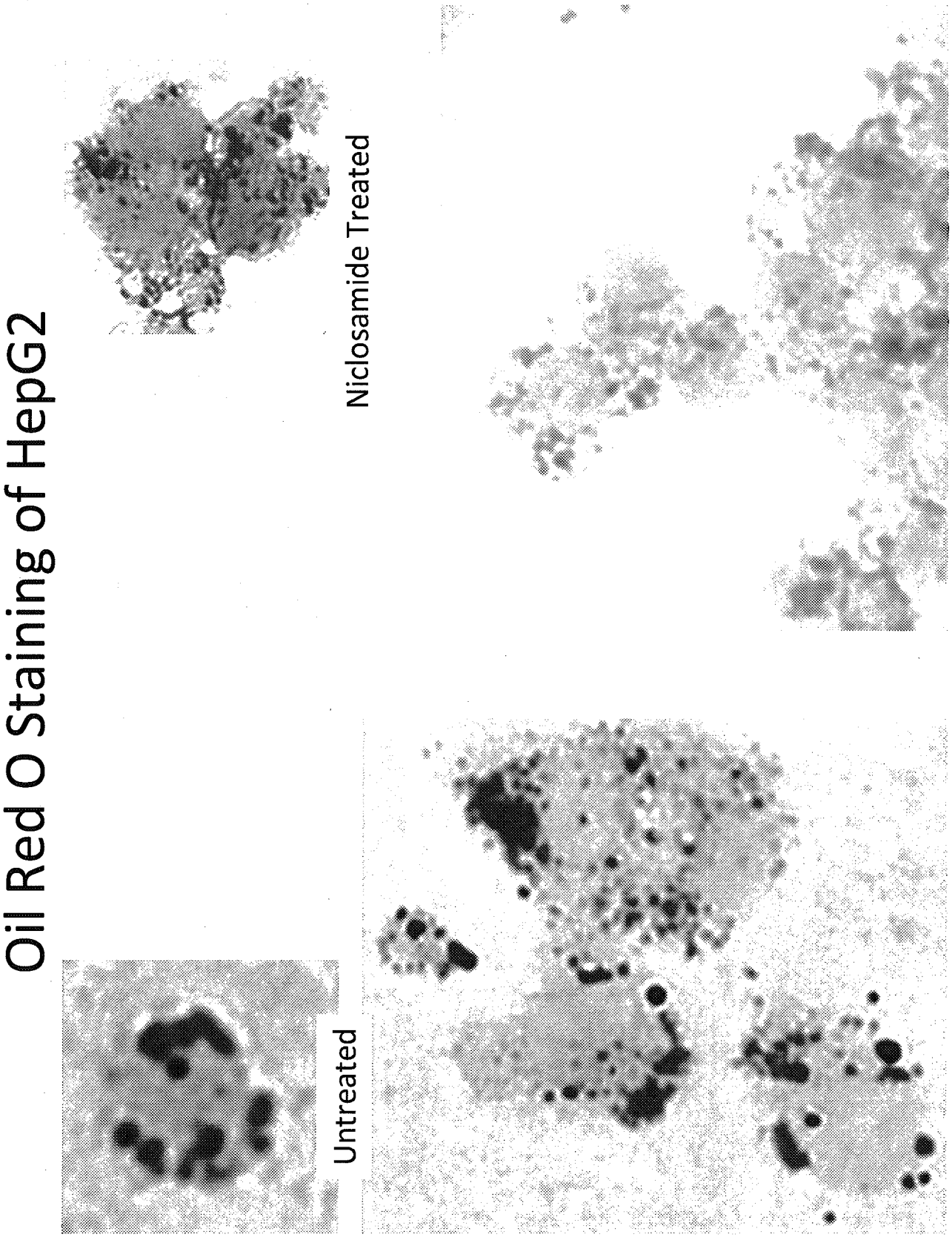
Oil Red O Staining of HepG2
Niclosamide Treated
Untreated